Q-band oscillator at 49GHz for broadband photonic microwave frequency conversion based on a Kerr soliton crystal micro-comb

David Moss (dmoss@swin.edu.au)
Swinburne University of Technology
mengxi tan
Swinburne University of Technology
xingyuan xu
Swinburne University of Technology

Research Article

Keywords: Microwave photonics, microwave frequency converters, Kerr optical comb

Posted Date: August 2nd, 2021

DOI: https://doi.org/10.21203/rs.3.rs-769776/v1

Abstract

We report a broadband microwave frequency converter based on a coherent Kerr optical micro-comb generated by an integrated micro-ring resonator. The coherent micro-comb displays features that are consistent with soliton crystal dynamics with an FSR of 48.9-GHz. We use this to demonstrate a high-performance millimeter-wave local oscillator at 48.9-GHz in the Q-band for microwave frequency conversion. We experimentally verify the microwave performance up to 40 GHz, achieving a ratio of −6.8 dB between output RF power and IF power and a spurious suppression ratio of > 43.5 dB. The experimental results show good agreement with theory and verify the effectiveness of microwave frequency converters based on coherent optical micro-combs, with the ability to achieve reduced size, complexity, and potential cost.

Introduction

Microwave frequency conversion for signal transmission or processing is a key processing block in radio-over-fibre (RoF) systems, beamforming and radio frequency communication networks [1-4]. As compared with electrical approaches that are subjected to the electrical bandwidth bottleneck [5, 6], photonic microwave frequency converters [7-9] could offer many competitive advantages including large bandwidth, high isolation, and strong immunity to electromagnetic interference, and so are promising solutions to meet with the ever-increasing demands for improved processing speed and performance.

Photonic microwave frequency converters are generally achieved by modulating an input microwave or radio frequency (RF) signal (with angular frequency ω_{RF}) and a local oscillator (LO) signal (with angular frequency ω_{LO}) onto an optical carrier and beat them upon photo-detection to produce the target intermediate frequency (IF) signal (with an angular frequency of $\omega_{IF} = \omega_{LO} \pm \omega_{RF}$). Many approaches to implement photonic microwave frequency converters have been reported, including those based on cascaded or parallel intensity modulators [7-12] and phase modulators [13]. Although diverse functions have been demonstrated for these frequency converters, they face limitations brought about by the external electrical LO sources, which suffer from the significantly increased cost and size for multi-stage frequency multiplication and the greatly degraded spectral purity at high frequencies, thus facing huge challenges to operate at high frequencies >40 GHz. Optoelectronic oscillators can address these limitations [14, 15], but are still subjected to the limited operational bandwidth caused by the electrical components (e.g., electrical amplifiers and narrow-band filters) and bulky system size involving fibre spools [16], for example.

Kerr optical micro-combs [17-24], particularly those in CMOS-compatible platforms [25-30], can offer many distinctive advantages to perform as an equivalent LO source for photonic microwave frequency converters. This includes the ability to generate high-frequency electrical signals ranging from 10 GHz up to 500 GHz (determined by the comb spacing), a high spectral purity enabled by the ultra-high coherence

of the generated states (e.g., Turing patterns, solitons, soliton crystals etc.), and a greatly reduced footprint (chip-scale) and complexity.

Here, we report a broadband LO-free photonic microwave frequency converter based on an integrated Kerr micro-comb source. Coherent micro-combs with a 48.9-GHz free spectral range (FSR) are generated by a high-Q micro-ring resonator (MRR) and serve as an equivalent millimeter-wave LO for microwave frequency conversion, thus eliminating the need of electronic LO sources and enabling wideband microwave frequency conversion within a greatly reduced potential footprint and cost. Meanwhile the optical parametric oscillation enables pure LO generation with a high frequency up to 48.9-GHz and even higher by utilizing multiple-FSR-spaced comb lines, thus enabling ultra-wideband microwave frequency conversion up to the U-band (40 to 60 GHz), which is extremely challenging for traditional photonic or electrical frequency convertors. In our experiments, the performance of the photonic microwave frequency converter is characterized at RF frequencies up to 40 GHz, achieving a ratio of −6.8 dB between output RF power and IF power, and a spurious suppression ratio of > 43.5 dB. This microcomb based photonic microwave frequency converter, with an ultra-high frequency photonic LO and greatly reduced system size, complexity, and potential cost, is a promising candidate for frequency conversion in modern radar and RoF systems.

Principle

Figure 1 shows a schematic diagram of the LO-free photonic microwave frequency converter. Coherent optical frequency combs were generated in an integrated MRR, which was pumped by a continuous-wave (CW) laser amplified by an erbium-doped fibre amplifier, with the polarization adjusted via a polarization controller to optimize the power coupled into the MRR. When the pump wavelength was swept across one of the MRR resonances with the pump power high enough to provide sufficient parametric gain, optical parametric oscillation occurred, ultimately generating Kerr optical combs with a spacing equal to the FSR of the MRR (~48.9 GHz). By properly setting the pump power and wavelength detuning, we succeeded in operating the Kerr optical micro-comb in a high coherence state, with a spectral output consistent with operation in the soliton crystal regime [24] that exhibits high coherence and low RF intensity noise. The low-noise micro-comb served as a high-performance millimeter-wave LO source for microwave frequency conversion, with the added benefits of significantly reduced complexity, device footprint, and potential cost. Moreover, the 48.9 GHz comb spacing also enabled an ultra-broad bandwidth for photonic microwave frequency conversion from the L-band to the U-band.

An optical bandpass filter was employed to select two adjacent comb lines from the coherent Kerr comb source for photonic microwave frequency conversion, and the optical field can be written as: **see formula 1 in the supplementary files section.**

where E_0 is the amplitude of the selected optical comb lines, ω and $(\omega+\omega_{LO})$ are the angular frequencies, with ω_{LO} denoting the angular frequency interval between them. The two comb lines were then modulated

by an RF input ($V_{RF} \cdot \cos\omega_{RF} t$) via a Mach-Zehnder modulator, to produce an optical field given by **see formula 2 in the supplementary files section.**

where $\varphi = \pi V_{dc} / V_{\pi}$ is the phase shift induced by the DC bias voltage, $\gamma = \pi V_{RF} / V_{\pi}$ is the modulation index, with V_{dc} and V_{π} denoting the DC voltage and the half-wave voltage, respectively.

Finally, the optical signals were amplified and converted back into electrical domain by a photodetector. With the Mach-Zehnder modulator biased at quadrature, the output electrical signal can be expressed as **see formula 3 in the supplementary files section.**

where J denotes the Bessel function of the first kind. As reflected by the above equation, photonic microwave frequency conversion can be achieved in this manner, with the angular frequency of the output IF signal given by ($\omega_{RF} + \omega_{LO}$) or ($\omega_{LO} - \omega_{RF}$). We note that spurious frequencies are also generated, including ($\omega_{LO} - 2\omega_{RF}$) = ($2\omega_{IF} - \omega_{LO}$) that appeared in our experiments.

Experiment

The MRR used to generate the Kerr optical comb (Fig. 2(a)) was fabricated on a high-index doped silica glass platform using CMOS-compatible fabrication processes [31-38]. First, high-index (n = ~1.7 at 1550 nm) doped silica glass films were deposited using plasma enhanced chemical vapour deposition, then patterned by deep ultraviolet photolithography and etched via reactive ion etching to form waveguides with exceptionally low surface roughness. Finally, silica (n = ~1.44 at 1550 nm) was deposited as an upper cladding. The advantages of our platform for optical micro-comb generation include ultra-low linear loss (~0.06 dB$\cdot$cm^{-1}), a moderate nonlinear parameter (~233 W$^{-1}\cdot$km^{-1}), and in particular negligible nonlinear loss up to extremely high intensities (~25 GW$\cdot$cm^{-2}). The radius of the MRR was ~ 592 μm, corresponding to an FSR of ~0.4 nm or~48.9 GHz (Fig. 2(b)). The relatively small FSR of the MRR led to a comb spacing falling in the millimeter-wave region, bridging the gap between the frequency scales of on-chip optical micro-combs and microwave systems. The ultra-low loss of the MRR resulted in a Q factor of ~1.5 million (Fig. 2(c)). After packaging the device with fibre pigtails, the through-port insertion loss was ~1 dB, assisted by on-chip mode converters.

To generate coherent micro-combs, the CW pump power was amplified to ~30.5 dBm and the wavelength swept from blue to red. When the detuning between the pump wavelength and MRR's cold resonance wavelength became small enough such that the intracavity power reached a threshold, modulation instability driven oscillation was initiated [25]. Primary combs were generated with a spacing of multiple FSRs, determined mainly by the intra-cavity power and dispersion. The calculated parametric gain (Fig. 3(a)) could be controlled by varying the pump wavelength detuning, which in turn resulted in different spacings of the generated primary combs (Fig. 3(b), (c)) [39, 40].

As the detuning was changed further, distinctive 'fingerprint' optical spectra were observed (Fig. 4) which were similar to the spectral interference between tightly packed solitons in the cavity – so called "soliton

crystals" that have been reported [24]. The soliton crystal step in the measured transmission (Fig. 4(c)) and the dramatic reduction of the RF intensity noise (Fig. 4(d)) are hallmarks of coherent micro-combs. Therefore, the ~ 48.9 GHz-spaced coherent combs were able to serve as an equivalent LO source, reaching the millimetre-wave region (U band, 40 to 60 GHz) – a regime that is challenging to achieve using traditional electrical methods [15]. Moreover, the optical power of the two comb lines near ~1541 nm (selected for the photonic microwave frequency conversion in our experiment) reached over 2 dBm (Fig. 4(a), zoom-in view), and the power ratio of the pump to the comb lines was -11 dBm (Fig. 4(b)), which provided a relatively high link gain for the microcomb-based microwave signal processors [41-43].

By changing the pump power within ± 0.5 dB, a diverse range of spectra were observed, all displaying low RF noise, and all being indicative with different soliton crystal superstructures [44] (Fig. 4, Fig. 5). This not only enabled the generation of coherent micro-combs for photonic microwave frequency conversion, but also offered a range of different comb spectral shapes suited to different applications. The formation of high quality stable combs, potentially consisting of soliton crystals, was readily achievable using straightforward adiabatic pump wavelength sweeping. We found that it was not necessary to achieve a rigorous single soliton state in order to achieve high microwave frequency conversion performance — only that the chaotic regime needed to be avoided. This is important since there are a much wider range of coherent low RF noise states that are more readily accessible than just the single soliton state [31, 39]. We employed a TEC (Thermo-Electric Cooller) controller to stabilize the chip temperature and the generated soliton crystal states were stable for over 12 hours without stabilization (other than the TEC) or feedback.

To generate the equivalent photonic LO, two comb lines near ~1541 nm were filtered and modulated by RF signals (with 14 dBm power) with different frequencies ranging up to 40 GHz. The corresponding optical spectra are shown in Fig. 6 (a). Next, the optical signals were amplified to 12 dBm and converted back into electrical domain where the frequency mixing of the RF signal and the LO signal was achieved via photo-detection. Figure 6(b) shows the measured electrical spectral output of the IF signal. As the input RF frequency f_{RF} was varied from 40 GHz to 23 GHz (from the Ka-band to the X-band), the converted IF output ($f_{IF} = f_{LO} - f_{RF}$) varied from 8.9 GHz to 25.9 GHz (from the X-band to the Ka-band) with a power variation of < 5 dB, reflecting the broad operational bandwidth of our photonic microwave frequency converter.

Figure 7(a) shows the output electrical spectra when f_{RF} = 26 GHz, corresponding to an IF output of 22.9 GHz.

The electrical spectra in a 10-MHz span (Fig. 7(b)) exhibited a signal-to-noise ratio of > 70 dB, which further confirmed the low noise performance of the photonic microwave frequency converter. The output power ratio of the IF to RF signals reached −6.3 dB, while the conversion efficiency of the output IF relative to the input RF power was −36.4 dB, with the −30.3dB link gain included. The spurious suppression ratio (power ratio of the IF signal to the spurious signal at $2f_{IF} - f_{LO}$) was 43.5 dB.

The phase noise performance of the input RF signal at 26 GHz and an output IF signal at 20.89 GHz was also measured using an RF spectrum analyzer (Keysight N9010A), as shown in Fig. 7(c). Here the 20.89 GHz IF tone was the converted output of a 28 GHz RF tone, instead of the measured 26 GHz RF tone, for the phase noise measurement. Yet since a 2 GHz difference in the RF tone's frequency would not significantly vary its phase noise performance, the phase noise spectra measured here could still reflect the performance of our photonic LO. The phase noise spectrum of the IF signal shows low residue noise brought about by the photonic LO at offset frequencies from 20 kHz to 1 GHz, verifying the microcomb's low noise performance that is promising for ultra-high frequency photonic LO generation and thus wideband microwave frequency conversion.

We note that the deterioration in the IF phase noise for offset frequencies < 20 kHz can be optimized by stabilizing the pump power [45] and setting the detuning to the quiet operation point [46]. Further optimization would need to deal with other noise sources such as the relative intensity noise of the pump and the thermal refractive noise of the resonator [47].

The frequency relationship between f_{RF} and the measured f_{IF} is clearly shown in Fig. 8, together with the calculated $f_{LO} = f_{IF} + f_{RF}$ = 48.9 GHz. This verifies the generation of a millimeter-wave LO using our approach and indicates the potential for ultra-wideband microwave frequency conversion from the L- to U-bands (i.e., 0 to 60 GHz). Note that our approach is capable of achieving even higher frequencies through the use of multiple-FSR-spaced comb lines. However, we were experimentally limited in our measurement capability by the bandwidth of our electrical spectrum analyzer and the RF source. As shown in Fig. 9, the IF power had a linear dependence on the input RF power (with a slope of 1.02, saturating at 10 dBm) and the optical power received at the photodetector (with a slope of 1.98), which matches closely with the theoretical predictions of 1 and 2, respectively from Eq. 3.

For applications requiring further suppression of spurious frequencies (such as $2f_{IF} - f_{LO}$), the two comb lines can be separated into two paths, where one is modulated by a carrier-suppressed double-sideband format to generate photonic RF sidebands, and the other serves as the photonic LO sideband for frequency mixing. In addition, though the LO frequency was not tunable in this paper, recent advances in dual micro-comb generation [48-49] provide possibilities to achieve a frequency-tunable photonic LO for the microwave frequency converter. By changing the relative offsets of the two combs via thermal tuning, an almost unlimited range of photonic LO frequencies can be realized from sub-GHz to beyond even a terahertz.

Conclusion

We demonstrate a broadband LO-free photonic microwave frequency converter based on an integrated Kerr comb source. Coherent micro-combs with a 48.9-GHz spacing were generated by a high-Q MRR and served as an equivalent millimeter-wave LO for microwave frequency conversion, enabling microwave frequency conversion up to the U-band. We experimentally verified the photonic microwave frequency converter's performance for input RF frequencies up to 40 GHz, achieving a ratio of −6.8 dB between

output RF power and IF power and a spurious suppression ratio of > 43.5 dB. With an ultra-high frequency photonic LO and greatly reduced system size, complexity, and potential cost, this microcomb based photonic microwave frequency converter is attractive for frequency conversion in radar and RoF systems.

Declarations

Competing interests: The authors declare no competing interests.

References

1. J. Capmany and D. Novak, “Microwave photonics combines two worlds,” *Nat. Photonics,* vol. 1, no. 6, pp. 319-330, Jun. 2007.
2. J. P. Yao, “Microwave Photonics,” *J. Lightwave Technol.,* vol. 27, no. 1-4, pp. 314-335, Jan. 2009.
3. J. Azana, C. Madsen, K. Takiguchi, and G. Cincotti, “Guest editorial - Optical signal processing,” *J. Lightwave Technol.,* vol. 24, no. 7, pp. 2484-2486, Jul. 2006.
4. K. Xu, R. X. Wang, Y. T. Dai, F. F. Yin, J. Q. Li, Y. F. Ji, and J. T. Lin, “Microwave photonics: radio-over-fiber links, systems, and applications,” *Photonics Res.,* vol. 2, no. 4, pp. B54-B63, Aug. 2014.
5. Y. S. Gao, A. J. Wen, W. Zhang, Y. Wang, and H. X. Zhang, “Photonic Microwave and mm-Wave Frequency converter for Multichannel Fiber Transmission,” *J. Lightwave Technol.,* vol. 35, no. 9, pp. 1566-1574, May. 2017.
6. J. Wu, X. Xu, T. G. Nguyen, S. T. Chu, B. E. Little, R. Morandotti, A. Mitchell, and D. J. Moss, “RF photonics: an optical microcombs' perspective,” *IEEE J. Sel. Top. Quantum Electron.,* vol. 24, no. 4, pp. 1-20, Jul-Aug. 2018.
7. X. W. Yang, K. Xu, J. Yin, Y. T. Dai, F. F. Yin, J. Q. Li, H. Lu, T. Liu, and Y. F. Ji, “Optical frequency comb based multi-band microwave frequency conversion for satellite applications,” *Opt. Express,* vol. 22, no. 1, pp. 869-877, Jan. 2014.
8. W. Zhang, A. J. Wen, Y. S. Gao, X. Y. Li, and S. Shang, “Microwave photonic frequency conversion with high conversion efficiency and elimination of dispersion-induced power fading,” *IEEE Photonics J.,* vol. 8, no. 3, Jun. 2016.
9. J. Zhang, E. H. W. Chan, X. Wang, X. Feng, and B. Guan, “High conversion efficiency photonic microwave frequency converter with image rejection capability,” *IEEE Photonics J.,* vol. 8, no. 4, Aug. 2016.
10. R. Chuenchom, X. H. Zou, N. Schrinski, S. Babiel, M. F. Hermelo, M. Steeg, A. Steffan, J. Honecker, Y. Leiba, and A. Stohr, “E-band 76-GHz coherent RoF backhaul link using an integrated photonic frequency converter,” *J. Lightwave Technol.,* vol. 34, no. 20, pp. 4744-4750, Oct. 2016.
11. Z. Z. Tang and S. L. Pan, “Reconfigurable microwave photonic frequency converter with minimized path separation and large suppression of mixing spurs,” *Opt. Lett.,* vol. 42, no. 1, pp. 33-36, Jan. 2017.

12. T. W. Jiang, R. H. Wu, S. Yu, D. S. Wang, and W. Y. Gu, “Microwave photonic phase-tunable frequency converter,” *Opt. Express,* vol. 25, no. 4, pp. 4519-4527, Feb. 2017.
13. V. R. Pagan and T. E. Murphy, “Electro-optic millimeter-wave harmonic downconversion and vector demodulation using cascaded phase modulation and optical filtering,” *Opt. Lett.,* vol. 40, no. 11, pp. 2481-2484, Jun. 2015.
14. J. Y. Lee and J. I. Song, “Photonic frequency down-converter based on a frequency-doubling OEO using two cascaded EAMs,” *IEEE Photonic Tech. L.,* vol. 29, no. 18, pp. 1529-1532, Sep. 2017.
15. D. Zhu, S. L. Pan, S. H. Cai, and D. Ben, “High-performance photonic microwave downconverter based on a frequency-doubling optoelectronic oscillator,” *J. Lightwave Technol.,* vol. 30, no. 18, pp. 3036-3042, Sep. 2012.
16. X. Xu, J. Dai, Y. Dai, F. Yin, Y. Zhou, J. Li, J. Yin, Q. Wang, and K. Xu, “Broadband and wide-range feedback tuning scheme for phase-locked loop stabilization of tunable optoelectronic oscillators,” *Opt. Lett.,* vol. 40, no. 24, pp. 5858-5861, Dec. 2015.
17. W. Liang, D. Eliyahu, V. S. Ilchenko, A. A. Savchenkov, A. B. Matsko, D. Seidel, and L. Maleki, “High spectral purity Kerr frequency comb radio frequency photonic oscillator,” *Nat. Commun.,* vol. 6, Aug. 2015.
18. P. Del'Haye, A. Coillet, T. Fortier, K. Beha, D. C. Cole, K. Y. Yang, H. Lee, K. J. Vahala, S. B. Papp, and S. A. Diddams, “Phase-coherent microwave-to-optical link with a self-referenced microcomb,” *Nat. Photonics,* vol. 10, no. 8, pp. 516-520, Aug. 2016.
19. X. X. Xue, Y. Xuan, Y. Liu, P. H. Wang, S. Chen, J. Wang, D. E. Leaird, M. H. Qi, and A. M. Weiner, “Mode-locked dark pulse Kerr combs in normal-dispersion microresonators,” *Nat. Photonics,* vol. 9, no. 9, pp. 594-600, Sep. 2015.
20. J. S. Levy, A. Gondarenko, M. A. Foster, A. C. Turner-Foster, A. L. Gaeta, and M. Lipson, “CMOS-compatible multiple-wavelength oscillator for on-chip optical interconnects,” *Nat. Photonics,* vol. 4, no. 1, pp. 37-40, Jan. 2010.
21. L. Razzari, D. Duchesne, M. Ferrera, R. Morandotti, S. Chu, B. E. Little, and D. J. Moss, “CMOS-compatible integrated optical hyper-parametric oscillator,” *Nat. Photonics,* vol. 4, no. 1, pp. 41-45, Jan. 2010.
22. D. J. Moss, R. Morandotti, A. L. Gaeta, and M. Lipson, “New CMOS-compatible platforms based on silicon nitride and Hydex for nonlinear optics,” *Nat. Photonics,* vol. 7, no. 8, pp. 597-607, Aug. 2013.
23. H. Guo, M. Karpov, E. Lucas, A. Kordts, M. H. P. Pfeiffer, V. Brasch, G. Lihachev, V. E. Lobanov, M. L. Gorodetsky, and T. J. Kippenberg, “Universal dynamics and deterministic switching of dissipative Kerr solitons in optical microresonators,” *Nat. Phys.,* vol. 13, no. 1, pp. 94-102, Jan. 2017.
24. D. C. Cole, E. S. Lamb, P. Del'Haye, S. A. Diddams, and S. B. Papp, “Soliton crystals in Kerr resonators,” *Nat. Photonics,* vol. 11, no. 10, pp. 671-676, Oct. 2017.
25. A. Pasquazi, M. Peccianti, L. Razzari, D. J. Moss, S. Coen, M. Erkintalo, Y. K. Chembo, T. Hansson, S. Wabnitz, P. Del Haye, X. X. Xue, A. M. Weiner, and R. Morandotti, “Micro-Combs: A Novel Generation of Optical Sources”, *Physics Reports,* vol. 729, pp. 1-81, Jan. 2018.

26. M. Ferrera, L. Razzari, D. Duchesne, R. Morandotti, Z. Yang, M. Liscidini, J. E. Sipe, S. Chu, B. E. Little, and D. J. Moss, “Low-power continuous-wave nonlinear optics in doped silica glass integrated waveguide structures,” *Nat. Photonics,* vol. 2, no. 12, pp. 737-740, Dec. 2008.
27. M. Kues, C. Reimer, B. Wetzel, P. Roztocki, B. E. Little, S. T. Chu, T. Hansson, E. A. Viktorov, D. J. Moss, and R. Morandotti, “Passively mode-locked laser with an ultra-narrow spectral width,” *Nat. Photonics,* vol. 11, no. 9, pp. 608-608, Sep. 2017.
28. M. Ferrera, Y. Park, L. Razzari, B. E. Little, S. T. Chu, R. Morandotti, D. J. Moss, and J. Azana, “On-chip CMOS-compatible all-optical integrator,” *Nat. Commun.,* vol. 1, Jun. 2010.
29. X. Y. Xu, M. X. Tan, J. Y. Wu, T. G. Nguyen, S. T. Chu, B. E. Little, R. Morandotti, A. Mitchell, and D. J. Moss, “Advanced Adaptive Photonic RF Filters with 80 Taps Based on an Integrated Optical Micro-Comb Source,” *J. Lightwave. Technol.,* vol. 37, no. 4, pp. 1288-1295, Feb 15. 2019.
30. X. Xu, J. Wu, M. Shoeiby, T. G. Nguyen, S. T. Chu, B. E. Little, R. Morandotti, A. Mitchell, and D. J. Moss, “Reconfigurable broadband microwave photonic intensity differentiator based on an integrated optical frequency comb source,” *APL Photonics,* vol. 2, no. 9, pp. 096104, Sep. 2017.
31. A. Pasquazi, L. Caspani, M. Peccianti, M. Clerici, M. Ferrera, L. Razzari, D. Duchesne, B. E. Little, S. T. Chu, D. J. Moss, and R. Morandotti, “Self-locked optical parametric oscillation in a CMOS compatible microring resonator: a route to robust optical frequency comb generation on a chip,” *Opt. Express,* vol. 21, no. 11, pp. 13333-13341, Jun. 2013.
32. X. Xu, J. Wu, L. Jia, M. Tan, T. G. Nguyen, S. T. Chu, B. E. Little, R. Morandotti, A. Mitchell, and D. J. Moss, “Continuously tunable orthogonally polarized RF optical single sideband generator based on micro-ring resonators,” *Journal of Optics,* vol. 20, no. 11, pp. 115701. 2018.
33. X. Xu, J. Wu, M. Tan, T. G. Nguyen, S. T. Chu, B. E. Little, R. Morandotti, A. Mitchell, and D. J. Moss, “Orthogonally Polarized RF Optical Single Sideband Generation and Dual-Channel Equalization Based on an Integrated Microring Resonator,” *J. Lightwave Technol.,* vol. 36, no. 20, pp. 4808-4818. 2018.
34. M. Peccianti, M. Ferrera, L. Razzari, R. Morandotti, B. E. Little, S. T. Chu, and D. J. Moss, “Subpicosecond optical pulse compression via an integrated nonlinear chirper,” *Opt. Express,* vol. 18, no. 8, pp. 7625-7633, Apr. 2010.
35. M. Ferrera, C. Reimer, A. Pasquazi, M. Peccianti, M. Clerici, L. Caspani, S. T. Chu, B. E. Little, R. Morandotti, and D. J. Moss, “CMOS compatible integrated all-optical radio frequency spectrum analyzer,” *Opt. Express,* vol. 22, no. 18, pp. 21488-21498, Sep. 2014.
36. X. Xu, M. Tan, J. Wu, T. G. Nguyen, S. T. Chu, B. E. Little, R. Morandotti, A. Mitchell, and D. J. Moss, “High performance RF filters via bandwidth scaling with Kerr micro-combs,” *APL Photonics,* vol. 4, no. 2, pp. 026102. 2019.
37. X. Xu, J. Wu, T. G. Nguyen, T. Moein, S. T. Chu, B. E. Little, R. Morandotti, A. Mitchell, and D. J. Moss, “Photonic microwave true time delays for phased array antennas using a 49 GHz FSR integrated optical micro-comb source [Invited],” *Photonics Res,* vol. 6, no. 5, pp. B30-B36, May 1. 2018.

38. X. Xu, M. Tan, J. Wu, T. G. Nguyen, S. T. Chu, B. E. Little, R. Morandotti, A. Mitchell, and D. J. Moss, “High performance RF filters via bandwidth scaling with Kerr micro-combs,” *APL Photonics,* vol. 4, no. 2, pp. 026102. 2019.
39. S. Coen, H. G. Randle, T. Sylvestre, and M. Erkintalo, “Modeling of octave-spanning Kerr frequency combs using a generalized mean-field Lugiato-Lefever model,” *Opt. Lett.,* vol. 38, no. 1, pp. 37-39, Jan. 2013.
40. Y. K. Chembo and C. R. Menyuk, “Spatiotemporal Lugiato-Lefever formalism for Kerr-comb generation in whispering-gallery-mode resonators,” *Phys. Rev. A.,* vol. 87, no. 5, May. 2013.
41. X. Xu, J. Wu, T. G. Nguyen, M. Shoeiby, S. T. Chu, B. E. Little, R. Morandotti, A. Mitchell, and D. J. Moss, “Advanced RF and microwave functions based on an integrated optical frequency comb source,” *Opt. Express,* vol. 26, no. 3, pp. 2569-2583, Jan. 2018.
42. T. G. Nguyen, M. Shoeiby, S. T. Chu, B. E. Little, R. Morandotti, A. Mitchell, and D. J. Moss, “Integrated frequency comb source-based Hilbert transformer for wideband microwave photonic phase analysis,” *Opt. Express,* vol. 23, no. 17, pp. 22087-22097, Aug. 2015.
43. X. Xu, J. Wu, T. G. Nguyen, S. Chu, B. Little, A. Mitchell, R. Morandotti, and D. J. Moss, “Broadband RF Channelizer based on an Integrated Optical Frequency Kerr Comb Source,” *J. Lightwave Technol.,* vol. 36, no. 19, pp. 7, 2018. 2018.
44. W. Q. Wang, Z. Z. Lu, W. F. Zhang, S. T. Chu, B. E. Little, L. R. Wang, X. P. Xie, M. L. Liu, Q. H. Yang, L. Wang, J. G. Zhao, G. X. Wang, Q. B. Sun, Y. S. Liu, Y. S. Wang, and W. Zhao, “Robust soliton crystals in a thermally controlled microresonator,” *Opt. Lett.,* vol. 43, no. 9, pp. 2002-2005, May. 2018.
45. T. Herr, V. Brasch, J. D. Jost, C. Y. Wang, N. M. Kondratiev, M. L. Gorodetsky, and T. J. Kippenberg, “Temporal solitons in optical microresonators,” *Nat. Photonics,* vol. 8, no. 2, pp. 145-152, Feb. 2014.
46. X. Yi, Q. F. Yang, X. Y. Zhang, K. Y. Yang, X. B. Li, and K. Vahala, “Single-mode dispersive waves and soliton microcomb dynamics,” *Nat. Commun.*, vol. 8, Mar 23. 2017.
47. G. Huang, E. Lucas, J. Liu, A. S. Raja, G. Lihachev, M. L. Gorodetsky, N. J. Engelsen, and T. J. Kippenberg, “Thermorefractive noise in silicon-nitride microresonators,” *Physical Review A*, vol. 99, no. 6, pp. 061801, 06/24/. 2019.
48. A. Dutt, C. Joshi, X. C. Ji, J. Cardenas, Y. Okawachi, K. Luke, A. L. Gaeta, and M. Lipson, “On-chip dual-comb source for spectroscopy,” *Sci. Adv.,* vol. 4, no. 3, Mar. 2018.
49. M. G. Suh, Q. F. Yang, K. Y. Yang, X. Yi, and K. J. Vahala, “Micro-resonator soliton dual-comb spectroscopy,” *Science*, vol. 354, no. 6312, pp. 600-603, Nov. 2016.

Figures

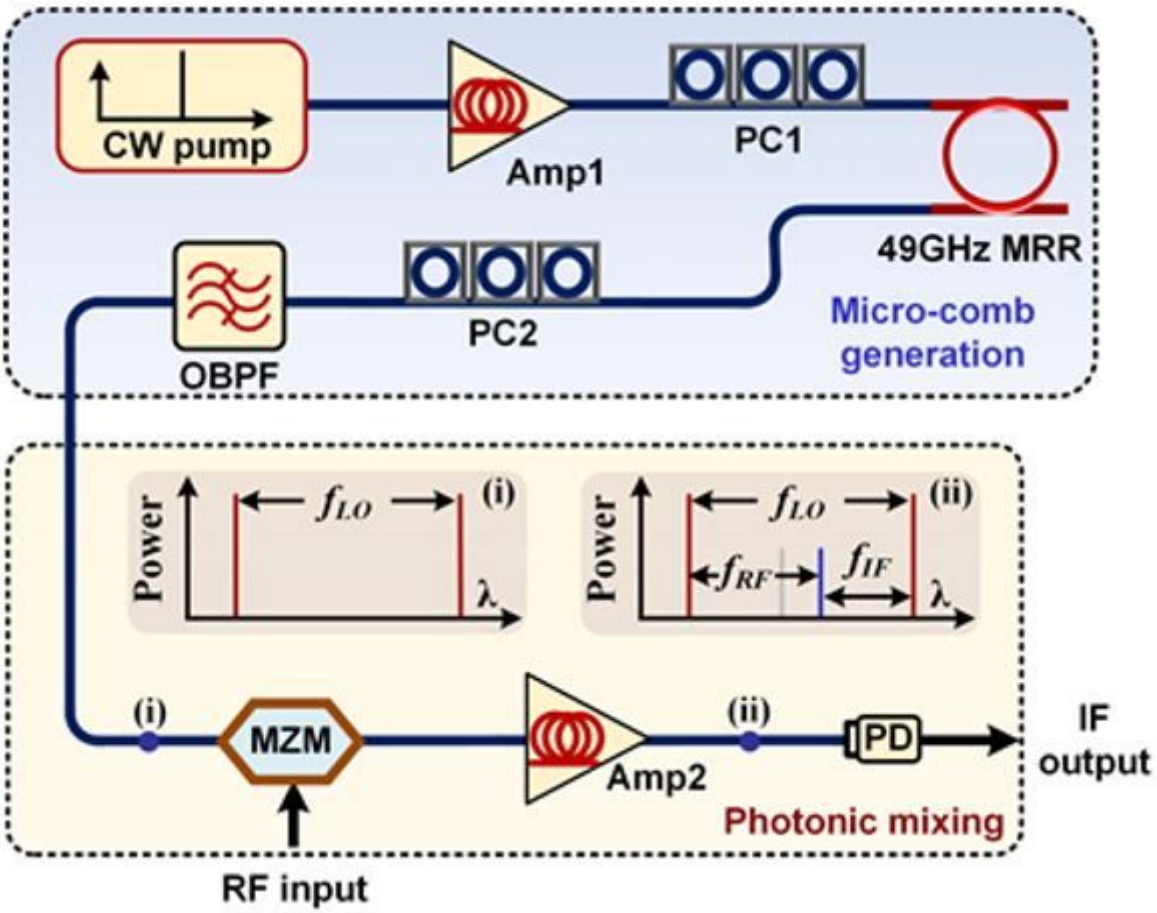

Figure 1

Schematic diagram of the LO-free photonic microwave frequency converter based on an integrated optical micro-comb source. Amp: erbium-doped fibre amplifier. PC: polarization controller. MRR: micro-ring resonator. OBPF: optical bandpass filter. MZM: Mach-Zehnder modulator. PD: photodetector.

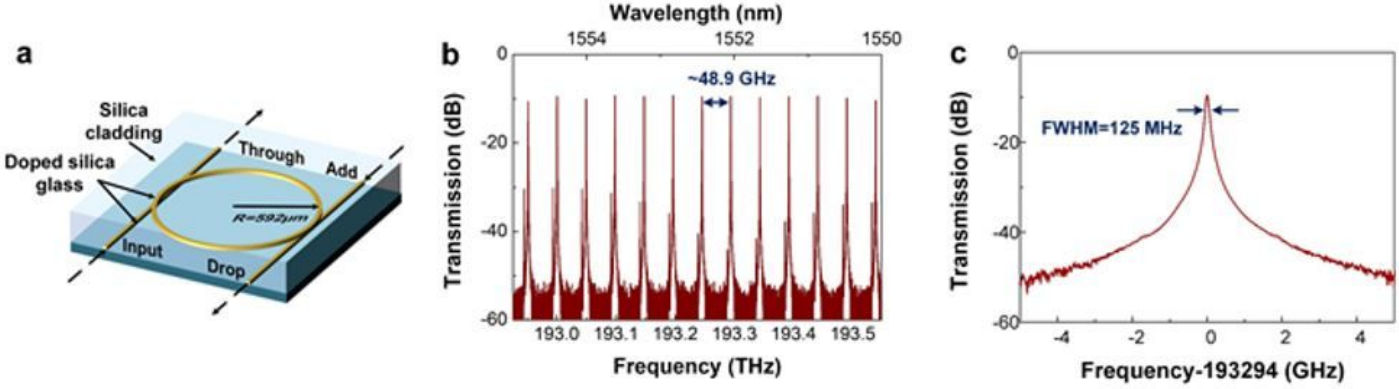

Figure 2

(a) Schematic illustration of the 48.9 GHz-FSR MRR. (b) Drop-port transmission spectrum of the integrated MRR with a span of 5 nm, showing an FSR of 48.9 GHz, and (c) a resonance at 193.294 THz with a full-width at half-maximum (FWHM) of ~125 MHz, corresponding to a Q factor of ~1.55×106.

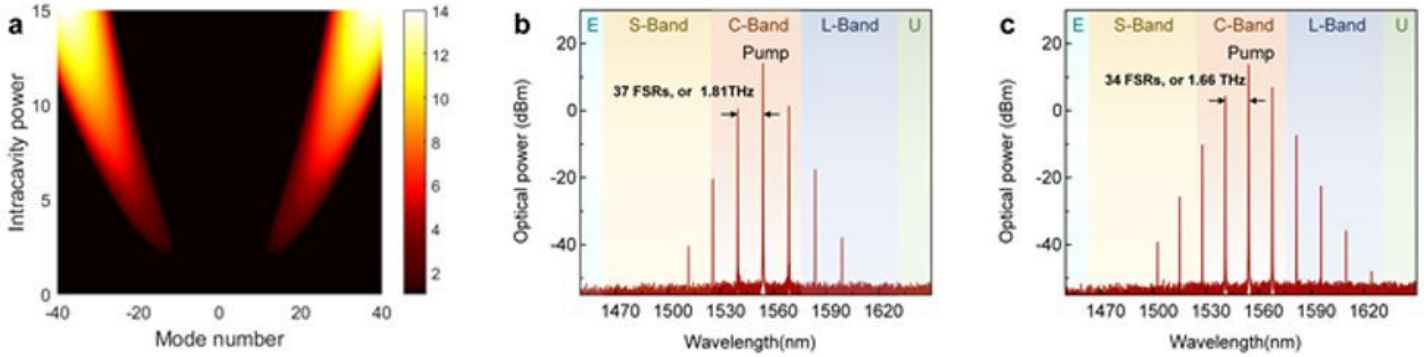

Figure 3

(a) Simulated parametric gain with linear scales and normalized units. Measured optical spectra of the primary combs with spacings of (b) 1.81 THz and (c) 1.66 THz.

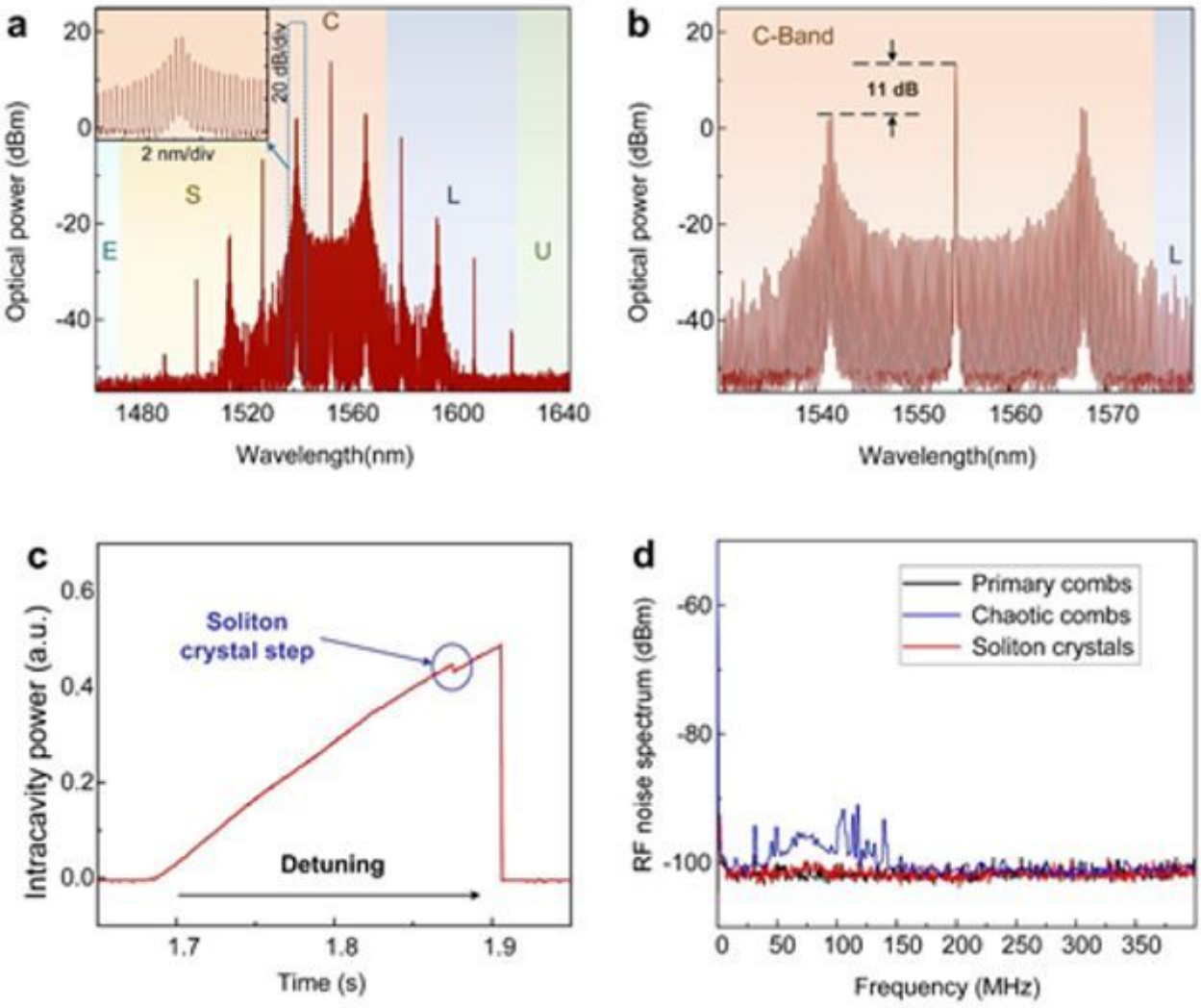

Figure 4

Measured optical spectrum of the generated micro-comb with a span of (a) 200 nm and (b) 50 nm. (c) Transmission of the pumping resonance and (d) the RF spectra corresponding to different regimes of micro-comb dynamics.

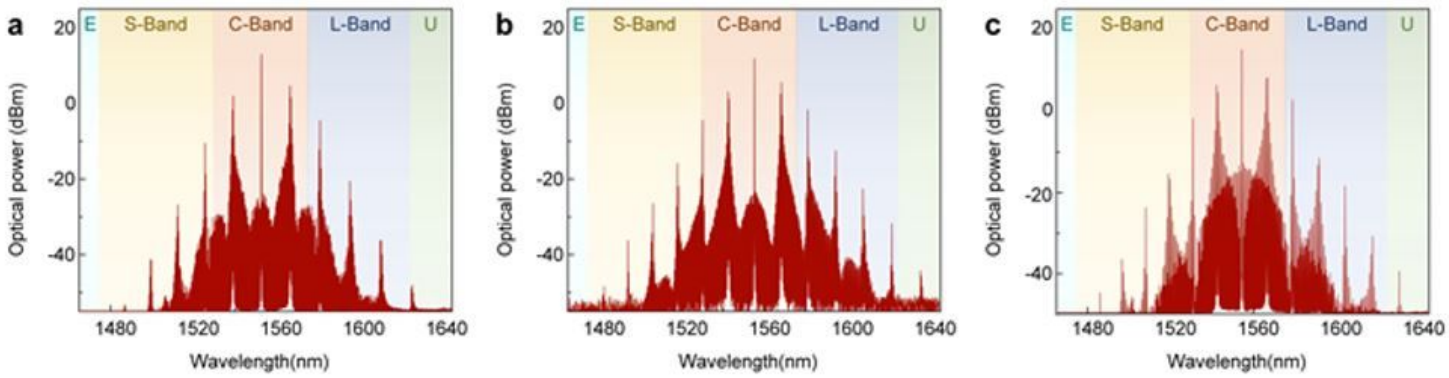

Figure 5

Optical spectra of the generated micro-combs showing different superstructures reminiscent of soliton crystals.

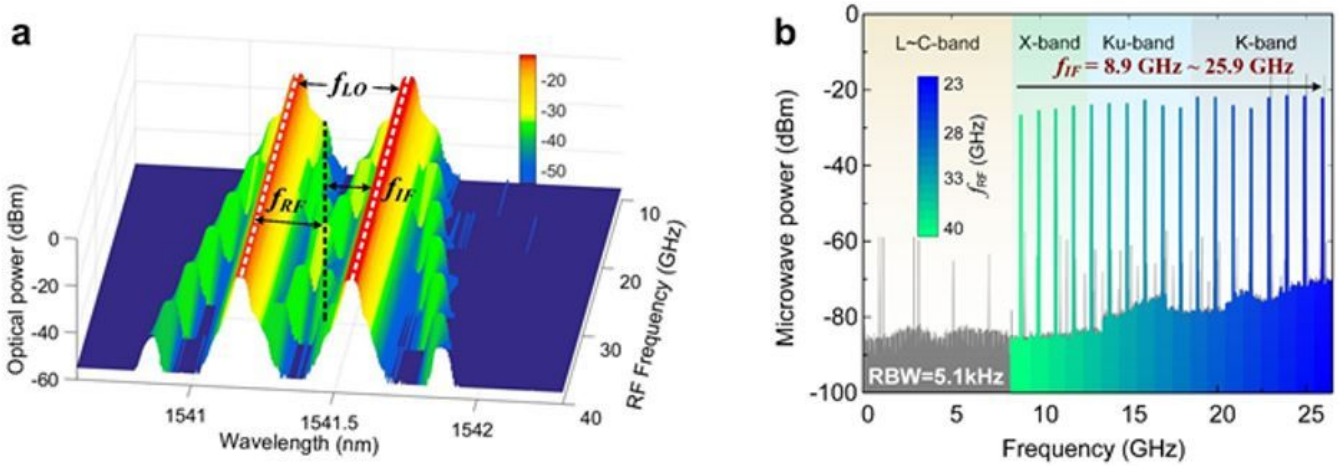

Figure 6

Measured (a) optical spectra of the equivalent photonic LO and (b) output IF electrical spectra, with the input RF frequency fRF varying from 40 GHz to 23 GHz.

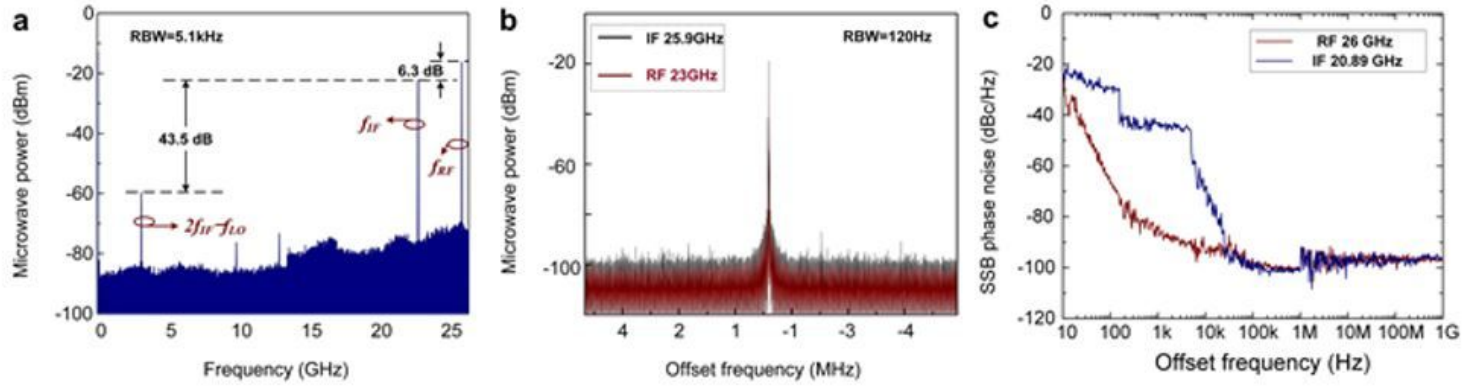

Figure 7

Measured (a) output electrical spectra of the photonic microwave frequency converter with fRF = 26 GHz, (b) electrical spectra of the input RF signal and output IF signal in a span of 10 MHz, and (c) phase noise spectra of the input RF signal at 26 GHz and the IF signal at 20.89 GHz.

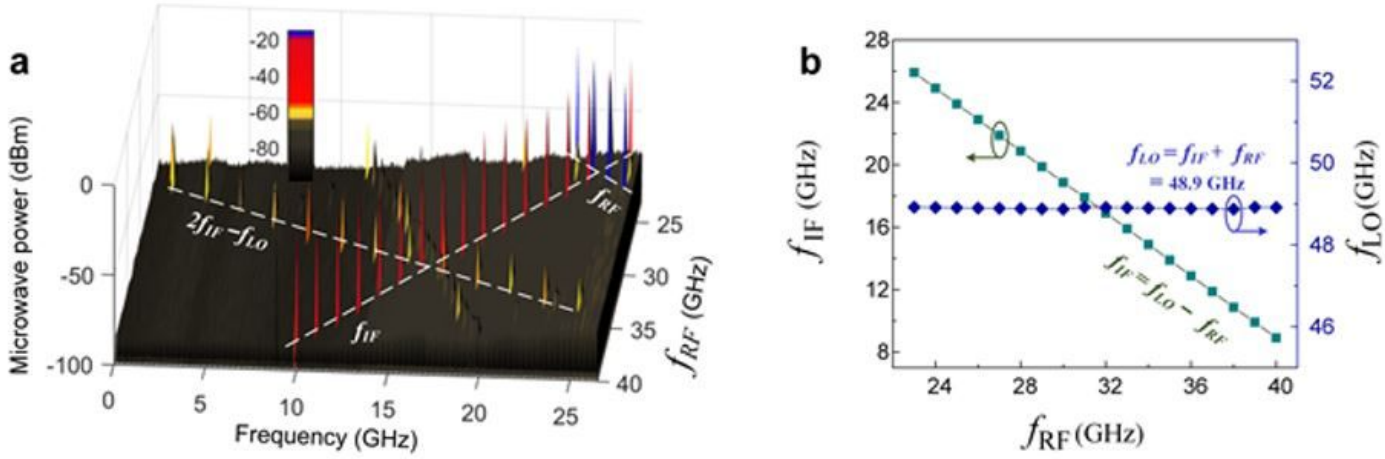

Figure 8

(a) Measured output electrical spectra of the photonic microwave frequency converter with input RF frequency fRF varying from 40 GHz to 23 GHz. (b) Extracted fIF and calculated fLO = fIF + fRF = 48.9 GHz.

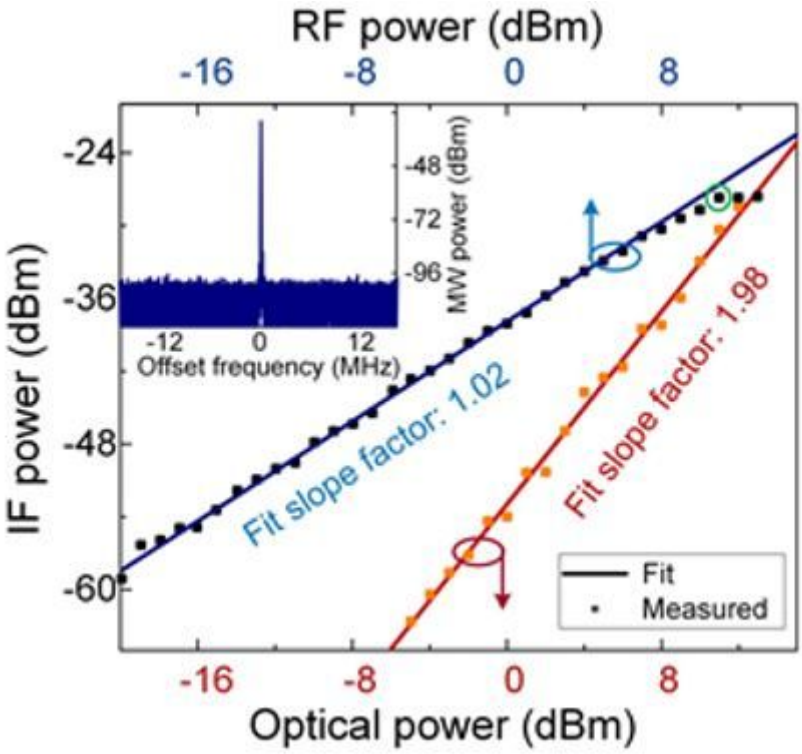

Figure 9

Two stacked plots of measured IF power for different input RF power and received optical power at the photodetector, respectively. The RF and optical power was fixed at 14 dBm and 12 dBm, respectively, when varying the other.

Supplementary Files

This is a list of supplementary files associated with this preprint. Click to download.

- formulas.docx